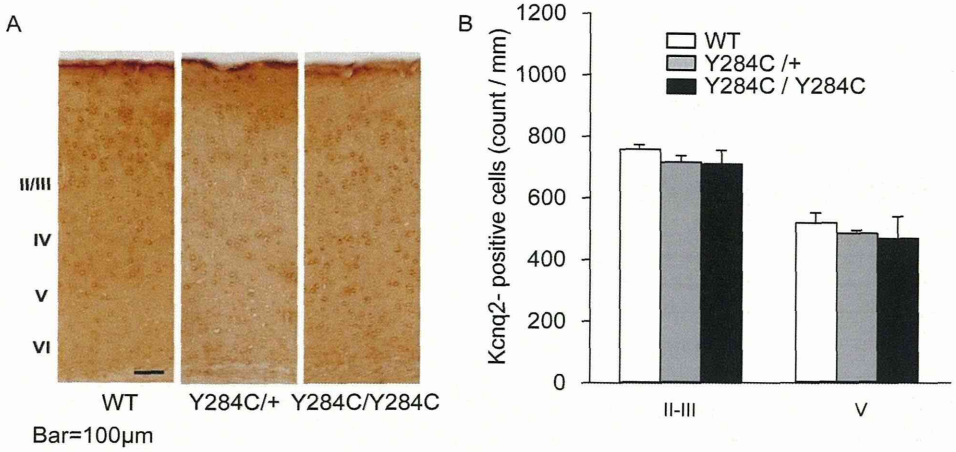

Figure 4. Morphological studies. (A) Light micrographs of $K_v7.2$ immunoreactivity in the sensorimotor cortex. Note the immunostained neuronal cell bodies in layers II to VI. (B) Cell count of $K_v7.2$-immunopositive neurons in layers II/III and V in the frontal cortices of wildtype, heterozygous, and homozygous Y284C mice. No differences were noted.
doi:10.1371/journal.pone.0088549.g004

post-hoc, wildtype *vs.* Y284C/Y284C, $P<0.01$ by Tukey-Kramer test. 10-week-old, −60 mV: wildtype = 36.2±6.3 pA (n = 15); Y284C/+ = 18.0±1.6 pA (n = 12); Y284C/Y284C = 17.7±1.7 pA (n = 9); $F = 4.72$, $P = 0.017$ by one-way ANOVA, post-hoc, wildtype *vs.* Y284C/+ and wildtype *vs.* Y284C/Y284C, $P<0.05$ by Tukey-Kramer test. These data indicate attenuation of the M-current in *Kcnq2* mutant mice.

Discussion

Advantages of the kick-in system

The kick-in system provides a solution for the problems associated with conventional knock-in technology. A comparison of both, the kick-in system and conventional knock-in technology, is shown in Figure 1. Conventional knock-in technology is a highly time- and cost-consuming undertaking that is primarily limited by resources, making the generation of multiple lines difficult. Any additional genetic alterations, even if situated near a previously examined change, require full-scale repetition of all previously invested effort, which complicates simultaneous analysis of many potentially interesting genetic variations. Side-by-side comparison of multiple knock-in mouse lines is therefore rare.

Contrary to the conventional knock-in technology, our kick-in system has been built on modified Cre/*lox* technology [21,22]. The recombination efficiency of our system is ~100% [11], whereas homologous recombination in the conventional strategy is as low as $1:10^5$ [23]. The kick-in system first establishes ES cells with recombination sites enveloping the target genomic region. These acceptor ES cells then serve as a platform for the development of animals with genetic alterations within the target region. Maintenance of the acceptor ES cells requires no more than standard tissue culture procedures. Target region knock-in mice from the acceptor ES cells were obtained within 8 weeks. Development of genetically altered animals can therefore proceed at previously impossible rates, making the side-by-side comparison of multiple animal lines feasible. This constitutes a significant step forward for basic research, which, up to this point, focused mainly on examining a single, "most important" variant of a protein, one at a time.

The kick-in, of course, does not stand alone when it comes to improvements in knock-in technology. There are various other knock-in modifications that provide significant advances over the traditional knock-in approach, such as the CRISPR/Cas system [24] and TALEN [25]. The CRISPR/Cas approach, for example, allows generation of knock-in mice within 4 weeks [26], but it requires a Protospacer Adjacent Motif, which limits the boundaries of the knock-in, while the kick-in accommodates a large target region.

Validity of the Kick-in System

Our mutant mouse lines demonstrate the validity of the kick-in system. We found no evidence of morphological or behavioral changes. Neuronal excitability, on the other hand, was elevated as revealed by EEG analysis and PTZ challenge. These findings compare to those gathered in mice produced with conventional *Kcnq2* knock-in technology. Singh *et al.* generated A306T mutant knock-in mice and examined them very closely. In their study, five A306T homozygous mice showed at least one forelimb and hindlimb tonic extension between P20 and P40, and all the mice died either immediately after birth or between P23 and P32 [9]. Although we did not observe spontaneous seizures in our A306T homozygotes, all of our mice similarly died at a young age. Interestingly, our Y284C homozygotes showed spontaneous forelimb and hindlimb clonus in addition to myoclonic seizures. Whether or not myoclonus can be a part of the phenotype in BFNE patients harboring the A306T or Y284C variation is uncertain, but patients with the A207T mutation reportedly do present with myoclonic jerks [27]. None of the Y284C homozygous mice died early, but 5 out of 17 (30%) homozygous mice perished during surgery for EEG analysis versus 3 out of 51 wildtype mice (6%) and 1 out of 50 heterozygous mice (2%), suggesting that Y284C homozygotic animals mice were more vulnerable during invasive brain surgery.

When challenged with the chemical convulsant PTZ, Y284C, and A306T animals showed elevated seizure susceptibility. These results are similar to the conventional knock-in A306T mice, in which the A306T heterozygotes had reduced electroconvulsive seizure thresholds, suggesting neuronal hyperexcitability [28]. Otto *et al.* proposed that increased seizure susceptibility and mortality after kindling relates to altered excitability in these animals [28]: PTZ and electroconvulsion both examine neuronal hyperexcitation, albeit through different pathways. Ties between neuronal hyperexcitability and *Kcnq2* deficiency are, of course, not

A

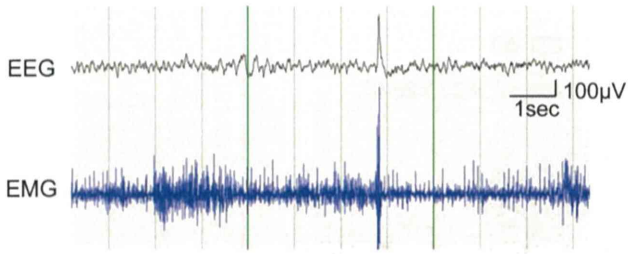

B

Score	Behavioral stage	EEG
0	No change in behavior	Baseline
1	Sudden behavioral arrest, motionless staring	High amplitude activities
2	Twitches, neck jerk, head to tail hiccup	Spikes, sharp waves
3	Minimal seizure with clonus of the head muscles to forelimbs, continuous tail elevation	Spikes or poly-spikes
4	Clonic seizure	Spike and wave discharges (SWD)
5	Tonic flexion, wild jumping, death	

C

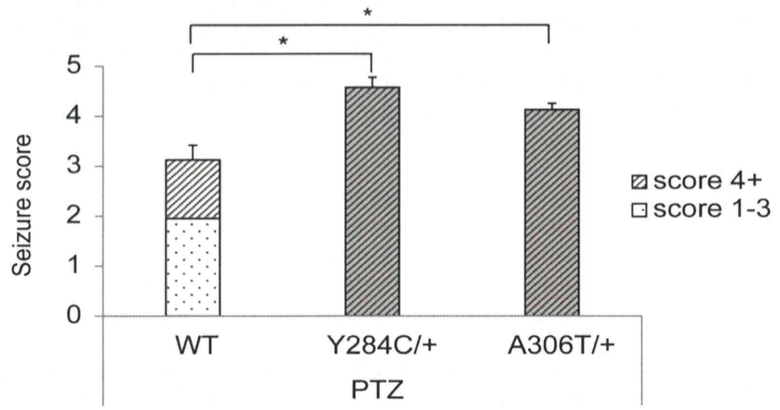

Figure 5. Behavioral analysis of Kcnq2 kick-ins. (A) Electroencephalography (EEG) with video monitoring revealed spontaneous myoclonic seizures with spike discharges in all Y284C homozygotes (n = 4). On average, the animals had 12 myoclonic seizures per hour in the daytime. (B) Modified Racine's scale. Behavioral criteria used to score the seizures in this study. Adopted and modified from Lüttjohann et al., 2009. All seizures scoring 4 or above were generalized. (C) Pentylenetetrazole/saline (PTZ) induced seizures in wildtype (white bar), Y284C, and A306T heterozygous mice (grey bars). The bar height represents the average seizure score; the hashed part of the bar represents the fraction of the animals that reached seizure score 4 and above. Asterisks denote $P<0.05$ (Tukey-Kramer test).
doi:10.1371/journal.pone.0088549.g005

new, as reported by Watanabe *et al.* who found hypersensitivity to PTZ [29].

In terms of neuronal hyperexcitability, A306T may produce stronger effects than Y284C, since A306T homozygotes died earlier than Y284C homozygotes. Direct comparative data between the human Y284C and A306T phenotype are not available [8], however, experiments in *Xenopus* oocytes revealed an I_M reduction by about 90% in homozygous A306T, while homozygous Y284C I_M was reduced by about 50%. Pseudo-heterozygous setups produce I_M reductions approximating 40% in both cases [30]. It is possible that the pronounced I_M effect is, at least in part, responsible for the premature death of the A306T homozygous animals. Singh *et al.* furthermore showed that CA1 neuronal I_M amplitudes from A306T heterozygous mice were no different from those measured in WT mice, but were significantly decreased in A306T homozygous mice at every potential tested [9]. The researchers concluded that the decrease in induced seizure threshold without changes in current amplitude in the heterozygous knock-in mice might be the result of faster deactivation kinetics seen in heterozygous mice. We also conducted direct electrophysiological analysis on Y284C brain slices, which show a significant reduction in I_M homozygous animals, in particular during strong depolarization at 4 and 10 weeks of age. Heterozygous brains also showed reductions in I_M, which may relate to these animals' lowered seizure threshold.

Since all experimental results confirm our approach's functionality, we conclude that the kick-in is a suitable technique to quickly generate a wide variety of genetic alterations. We see the kick-in as an enabler for phenotyping efforts of novel pathogenic and non-pathogenic alterations in an era where new genetic variation data become rapidly available. We furthermore present a new BFNE model, which will help advance our understanding of pediatric epilepsy by providing a platform for various functional analyses.

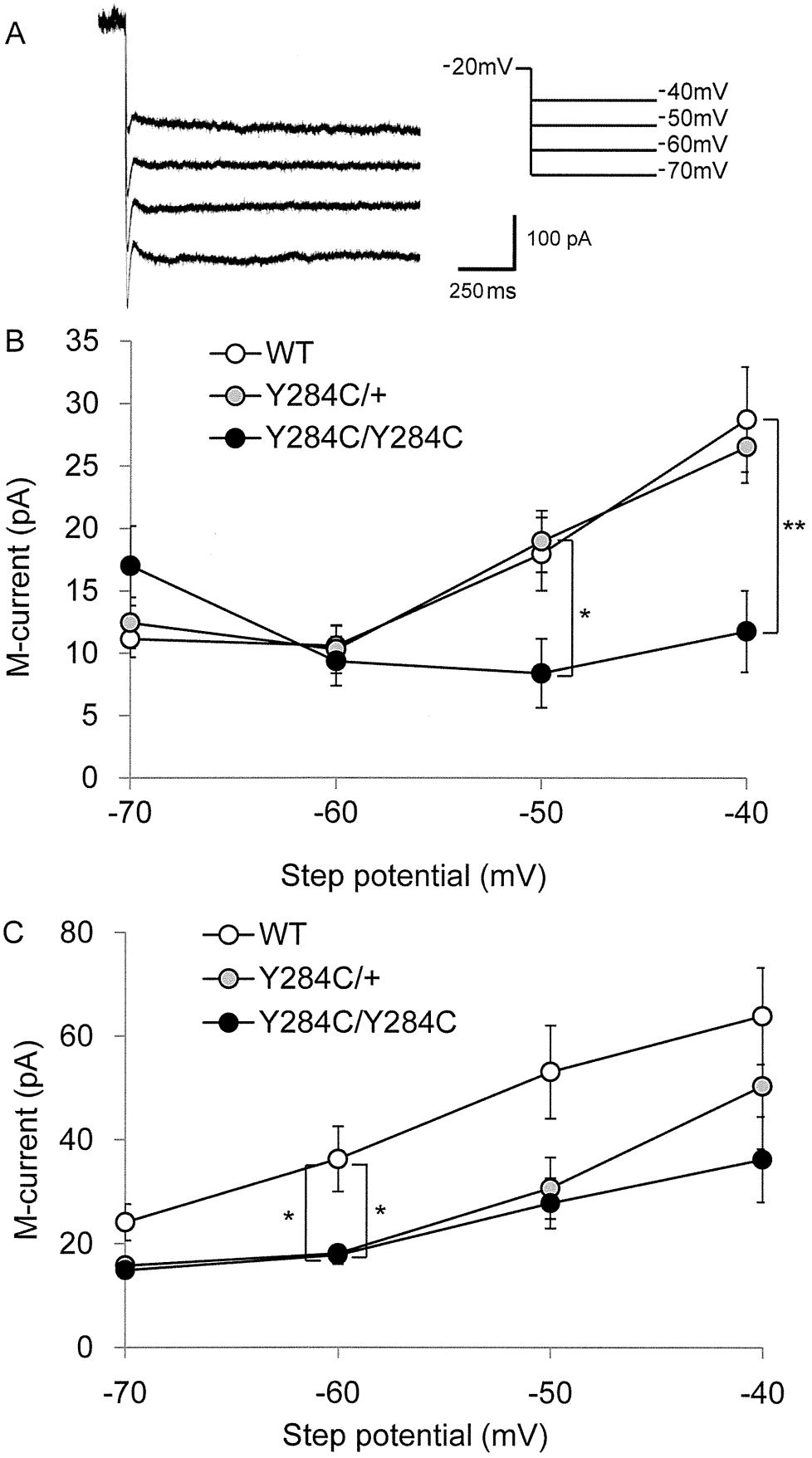
A
-20mV
-40mV
-50mV
-60mV
-70mV
100 pA
250 ms
B
WT
Y284C/+
Y284C/Y284C
M-current (pA)
Step potential (mV)
*
**
C
WT
Y284C/+
Y284C/Y284C
M-current (pA)
Step potential (mV)
*
*

Figure 6. Kcnq2 mutant brain slice electrophysiology. (A) Sample traces recorded from 10-week old Y284C heterozygous CA1 neurons in response to voltage steps to the indicated potential. (B, C) Voltage-dependence of M-current activation in wildtype (○), heterozygous (◍), and homozygous (●) Y284C mice at 4 weeks (B) and 10 weeks (C). Whole-cell perforated patched CA1 neurons were stepped to the indicated potential and back to −20 mV to determine tail current amplitudes. Significant I_M reductions were seen in Y284C homozygotes at 4 and 10 weeks, and in heterozygotes at 10 weeks at −60 mV ($P<0.05$, Tukey-Kramer test).
doi:10.1371/journal.pone.0088549.g006

Supporting Information

Figure S1 c-Fos based excitability measurements in the Kcnq2 mutants. c-Fos expression is a measure of prior cellular activity. Wildtype somatosensory cortex and dentate gyrus were indistinguishable from that of newborn Y284C homozygotes. By comparison, close examination of the dorsal hippocampus, a region commonly implicated in seizure disorders, revealed a clear and significant increase in c-Fos expression, which is indicative of cellular hyperactivity ($P<0.05$, Tukey-Kramer test).
(TIF)

Acknowledgments

We are grateful to Ms. Minako Yonetani, Ms. Akiyo Hamachi, all the members of Central Research Institute for the Molecular Pathomechanisms of Epilepsy, and all the students of the epilepsy group of Department of Physiology and Pharmacology, Fukuoka University for their support.

Author Contributions

Conceived and designed the experiments: MD KA SH. Performed the experiments: MD KA YM TA Y. Tanaka H. Kitamura FM Y. Tomonoh SY RS MI TU JY KM H. Kitaura. Analyzed the data: Y. Tomonoh. Contributed reagents/materials/analysis tools: MD KA FM KW RS MI JY KM SU H. Kitaura AK Y. Takano SH. Wrote the paper: Y. Tomonoh MD KA FM MI TU JY CL Y. Takano SH.

References

1. Hirose S, Mitsudome A, Okada M, Kaneko S, Epilepsy Genetic Study Group J (2005) Genetics of idiopathic epilepsies. Epilepsia 46 Suppl 1: 38–43.
2. Kaneko S, Okada M, Iwasa H, Yamakawa K, Hirose S (2002) Genetics of epilepsy: current status and perspectives. Neurosci Res 44: 11–30.
3. Ronen GM, Rosales TO, Connolly M, Anderson VE, Leppert M (1993) Seizure characteristics in chromosome 20 benign familial neonatal convulsions. Neurology 43: 1355–1360.
4. Vigevano F (2005) Benign familial infantile seizures. Brain Dev 27: 172–177.
5. Dedek K, Fusco L, Teloy N, Steinlein OK (2003) Neonatal convulsions and epileptic encephalopathy in an Italian family with a missense mutation in the fifth transmembrane region of KCNQ2. Epilepsy Res 54: 21–27.
6. Borgatti R, Zucca C, Cavallini A, Ferrario M, Panzeri C, et al. (2004) A novel mutation in KCNQ2 associated with BFNC, drug resistant epilepsy, and mental retardation. Neurology 63: 57–65.
7. Weckhuysen S, Mandelstam S, Suls A, Audenaert D, Deconinck T, et al. (2012) KCNQ2 encephalopathy: emerging phenotype of a neonatal epileptic encephalopathy. Ann Neurol 71: 15–25.
8. Singh NA, Charlier C, Stauffer D, DuPont BR, Leach RJ, et al. (1998) A novel potassium channel gene, KCNQ2, is mutated in an inherited epilepsy of newborns. Nat Genet 18: 25–29.
9. Singh NA, Otto JF, Dahle EJ, Pappas C, Leslie JD, et al. (2008) Mouse models of human KCNQ2 and KCNQ3 mutations for benign familial neonatal convulsions show seizures and neuronal plasticity without synaptic reorganization. J Physiol 586: 3405–3423.
10. Yagi T, Tokunaga T, Furuta Y, Nada S, Yoshida M, et al. (1993) A novel ES cell line, TT2, with high germline-differentiating potency. Anal Biochem 214: 70–76.
11. Araki K, Araki M, Yamamura K (2002) Site-directed integration of the cre gene mediated by Cre recombinase using a combination of mutant lox sites. Nucleic Acids Res 30: e103.
12. Berger SL, Chirgwin JM (1989) Isolation of RNA. Methods Enzymol 180: 3–13.
13. Luttjohann A, Fabene PF, van Luijtelaar G (2009) A revised Racine's scale for PTZ-induced seizures in rats. Physiol Behav 98: 579–586.
14. Otto JF, Yang Y, Frankel WN, White HS, Wilcox KS (2006) A spontaneous mutation involving Kcnq2 (Kv7.2) reduces M-current density and spike frequency adaptation in mouse CA1 neurons. J Neurosci 26: 2053–2059.
15. Araki K, Okada Y, Araki M, Yamamura K (2010) Comparative analysis of right element mutant lox sites on recombination efficiency in embryonic stem cells. BMC Biotechnol 10: 29.
16. Araki K, Araki M, Yamamura K (1997) Targeted integration of DNA using mutant lox sites in embryonic stem cells. Nucleic Acids Res 25: 868–872.
17. Dymecki SM (1996) Flp recombinase promotes site-specific DNA recombination in embryonic stem cells and transgenic mice. Proc Natl Acad Sci U S A 93: 6191–6196.
18. McLeod M, Craft S, Broach JR (1986) Identification of the crossover site during FLP-mediated recombination in the Saccharomyces cerevisiae plasmid 2 microns circle. Mol Cell Biol 6: 3357–3367.
19. VanElzakker M, Fevurly RD, Breindel T, Spencer RL (2008) Environmental novelty is associated with a selective increase in Fos expression in the output elements of the hippocampal formation and the perirhinal cortex. Learn Mem 15: 899–908.
20. Dragunow M, Faull R (1989) The use of c-fos as a metabolic marker in neuronal pathway tracing. J Neurosci Methods 29: 261–265.
21. Abremski K, Hoess R, Sternberg N (1983) Studies on the properties of P1 site-specific recombination: evidence for topologically unlinked products following recombination. Cell 32: 1301–1311.
22. Sauer B (1998) Inducible gene targeting in mice using the Cre/lox system. Methods 14: 381–392.
23. Doetschman T, Gregg RG, Maeda N, Hooper ML, Melton DW, et al. (1987) Targetted correction of a mutant HPRT gene in mouse embryonic stem cells. Nature 330: 576–578.
24. Horvath P, Barrangou R (2010) CRISPR/Cas, the immune system of bacteria and archaea. Science 327: 167–170.
25. Wefers B, Meyer M, Ortiz O, Hrabe de Angelis M, Hansen J, et al. (2013) Direct production of mouse disease models by embryo microinjection of TALENs and oligodeoxynucleotides. Proc Natl Acad Sci U S A 110: 3782–3787.
26. Wang H, Yang H, Shivalila CS, Dawlaty MM, Cheng AW, et al. (2013) One-step generation of mice carrying mutations in multiple genes by CRISPR/Cas-mediated genome engineering. Cell 153: 910–918.
27. Blumkin L, Suls A, Deconinck T, De Jonghe P, Linder I, et al. (2012) Neonatal seizures associated with a severe neonatal myoclonus like dyskinesia due to a familial KCNQ2 gene mutation. Eur J Paediatr Neurol 16: 356–360.
28. Otto JF, Singh NA, Dahle EJ, Leppert MF, Pappas CM, et al. (2009) Electroconvulsive seizure thresholds and kindling acquisition rates are altered in mouse models of human KCNQ2 and KCNQ3 mutations for benign familial neonatal convulsions. Epilepsia 50: 1752–1759.
29. Watanabe H, Nagata E, Kosakai A, Nakamura M, Yokoyama M, et al. (2000) Disruption of the epilepsy KCNQ2 gene results in neural hyperexcitability. J Neurochem 75: 28–33.
30. Schroeder BC, Kubisch C, Stein V, Jentsch TJ (1998) Moderate loss of function of cyclic-AMP-modulated KCNQ2/KCNQ3 K+ channels causes epilepsy. Nature 396: 687–690.

nature COMMUNICATIONS

ARTICLE

Received 18 Feb 2014 | Accepted 23 Jun 2014 | Published 22 Jul 2014

DOI: 10.1038/ncomms5501

Elfn1 recruits presynaptic mGluR7 in trans and its loss results in seizures

Naoko H. Tomioka[1,†], Hiroki Yasuda[2], Hiroyuki Miyamoto[3,4], Minoru Hatayama[1,5], Naoko Morimura[1], Yoshifumi Matsumoto[1], Toshimitsu Suzuki[6], Maya Odagawa[1], Yuri S. Odaka[1], Yoshimi Iwayama[7], Ji Won Um[8], Jaewon Ko[8], Yushi Inoue[9], Sunao Kaneko[10], Shinichi Hirose[11], Kazuyuki Yamada[12], Takeo Yoshikawa[7], Kazuhiro Yamakawa[6] & Jun Aruga[1,5]

GABAergic interneurons are highly heterogeneous, and much is unknown about the specification and functional roles of their neural circuits. Here we show that a transinteraction of Elfn1 and mGluR7 controls targeted interneuron synapse development and that loss of Elfn1 results in hyperactivity and sensory-triggered epileptic seizures in mice. Elfn1 protein increases during postnatal development and localizes to postsynaptic sites of somatostatin-containing interneurons (SOM-INs) in the hippocampal CA1 stratum oriens and dentate gyrus (DG) hilus. *Elfn1* knockout (KO) mice have deficits in mGluR7 recruitment to synaptic sites on SOM-INs, and presynaptic plasticity is impaired at these synapses. In patients with epilepsy and attention deficit hyperactivity disorder (ADHD), we find damaging missense mutations of *ELFN1* that are clustered in the carboxy-terminal region required for mGluR7 recruitment. These results reveal a novel mechanism for interneuron subtype-specific neural circuit establishment and define a common basis bridging neurological disorders.

[1] Laboratory for Behavioral and Developmental Disorders, RIKEN Brain Science Institute (BSI), Wako-shi, Saitama 351-0198, Japan. [2] Education and Research Support Center, Gunma University Graduate School of Medicine, Maebashi 371-8511, Japan. [3] Laboratory for Neurobiology of Synapse, RIKEN BSI, Wako-shi, Saitama 351-0198, Japan. [4] Precursory Research for Embryonic Science and Technology, Japan Science and Technology Agency, Saitama 332-0012, Japan. [5] Department of Medical Pharmacology, Nagasaki University Graduate School of Biomedical Sciences, Nagasaki 852-8523, Japan. [6] Laboratory for Neurogenetics, RIKEN BSI, Wako-shi, Saitama 351-0198, Japan. [7] Laboratory for Molecular Psychiatry, RIKEN BSI, Wako-Shi, Saitama 351-0198, Japan. [8] Department of Biochemistry, College of Life Science and Biotechnology, Yonsei University, Seoul 120-749, Korea. [9] National Epilepsy Center, Shizuoka Institute of Epilepsy and Neurological Disorders, Shizuoka 420-8688, Japan. [10] Department of Neuropsychiatry, Hirosaki University Graduate School of Medicine, Hirosaki 036-8216, Japan. [11] Department of Pediatrics, Fukuoka University School of Medicine, Fukuoka 814-0180, Japan. [12] Support Unit for Animal Experiments, RIKEN BSI, Wako-shi, Saitama 351-0198, Japan. † Present address: Department of Human Physiology and Pathology, Faculty of Pharma-Sciences, Teikyo University, Tokyo 173-8605, Japan. Correspondence and requests for materials should be addressed to J.A. (email: aruga@nagasaki-u.ac.jp).

GABAergic interneurons in the mammalian neocortex constitute a relatively small population in comparison to excitatory neurons, but are highly heterogeneous[1]. Recent studies have defined the properties of interneuron subtypes based on their morphology, functionality, molecular markers and origins[2,3]. Although interneurons are known to participate in local neural circuits in a subtype-specific manner, the molecular basis by which the connectivity of each interneuron is determined remains unclear. Furthermore, although GABAergic interneurons are proposed to be essential for excitatory and inhibitory balance[4], little is known of the behavioural and physiological pathology caused by the genetic dysfunction of neural circuitry that contains specific local interneurons.

Hippocampal interneurons are appropriate for addressing these issues because of their distinct and relatively well-characterized properties. Among them, oriens lacunosum moleculare (OLM) cells in the CA1 region and hilar perforant path-associated (HIPP) cells in the DG share the following features: they (1) innervate the distal dendrites of principal neurons (CA1 pyramidal neurons and DG granule neurons); (2) fire rhythmically at theta frequency[5,6]; (3) co-express somatostatin (SOM), neuropeptide Y and metabotropic glutamate receptor 1a (mGluR1a)[7–9]; and (4) are decorated by metabotropic glutamate receptor 7 (mGluR7)-containing presynaptic structures[10,11]. Furthermore, both OLM and HIPP cells are affected in several models of temporal lobe epilepsy, suggesting the clinical importance of this subset of interneurons[12,13].

The presynaptic mGluR7 in local circuits involving OLM and HIPP cells is considered to control brain excitability and higher cognitive function[14–17]. mGluR7 exists in the presynaptic active zone, and interestingly, the protein is differentially concentrated at the single synaptic terminal, depending on the nature of the postsynaptic neurons[10]. This finding suggests that some key molecules on OLM/HIPP cells trigger presynaptic mGluR7 accumulation. mGluR7 binds to the presynaptic scaffold protein PICK1 through its C terminus, and this interaction is essential for its presynaptic clustering[18,19] and suppression of seizures[15,16]. However, binding to PICK1 alone cannot explain the accumulation of mGluR7 onto specific interneurons. Although mGluR1a would seem to be a candidate postsynaptic determinant, this is not the case. The absence of mGluR1a does not affect the high level of mGluR7[10], suggesting the existence of an as-yet-unidentified molecule.

Here we show that the transmembrane protein Elfn1 (extracellular-leucine-rich repeat (LRR) fibronectin domain1)[20] in OLM cells is a critical postsynaptic component that induces mGluR7-positive presynaptic structures in excitatory neurons. The neurological phenotypes we observed in *Elfn1* knockout (KO) mice are strikingly similar to those of mGluR7-deficient mice, suggesting that the functions of Elfn1 and mGluR7 proteins are closely linked. Furthermore, in searching for *ELFN1* variants in patients with neurological disorders, we identified novel missense mutations that specifically impair the mGluR7-recruiting function of ELFN1 via its C-terminal domain. These findings raise the possibility that dysfunction of the ELFN1–mGluR7 complex is a critical contributor to neurological diseases.

Results

Elfn1 localizes to excitatory postsynapses on SOM-INs. Elfn1 is a presumptive type I transmembrane protein containing a LRR domain, a fibronectin type-III domain and a transmembrane domain (Fig. 1a)[20]. In mice, *Elfn1* is strongly expressed in interneurons of the hippocampus (hp) and cerebral cortex[20].

To visualize its protein distribution, we generated an anti-Elfn1 C terminus antibody that does not cross-react with Elfn2, which is another Elfn family protein (Supplementary Fig. 1a), and performed immunoblot (IB) (Fig. 1b – d) and immunofluorescence staining (Fig. 1e–g,j and Supplementary Fig. 1b). A subcellular fractionation analysis revealed that Elfn1 protein was highly enriched in the P2 membrane fraction (which contains myelin, synaptosomes and mitochondria); it was also recovered in the synaptosomal (LP1), synaptosomal plasma membrane (SPM) and postsynaptic density (PSD) fractions, but not in the synaptic vesicle-enriched fraction (LP2) (Fig. 1b). These results were consistent with a previous study indicating that Elfn1 localizes mostly to excitatory postsynaptic sites[21].

In the mouse whole brain lysate, Elfn1 was weakly detected during the first week after birth, and strongly detected during 2 to 8 weeks after birth (Fig. 1c). In adult brain, Elfn1 was strongly detected in the cerebral cortex, hp, habenular nuclei, septum, diagonal bands, anterior amygdaloid area, globus pallidus and medial forebrain bundles and moderately in the substantial nigra, ventral tegmental nucleus and interpeduncular nuclei (Fig. 1d,e and Supplementary Fig. 1b), which is largely consistent with the distribution of *Elfn1* mRNA[20,22]. In the hp, strong Elfn1 immunoreactivity was detected in the stratum oriens (SO) of the CA1 region, strata oriens and lacunosum of the CA3 region and hilus of the DG (Fig. 1e).

Elfn1 expression occurs in SOM-INs)[20,21]. In our culture system, 96% of the Elfn1-positive neurons were GAD67-positive ($n = 51$), whereas 35% of the GAD67-positive cells were Elfn1-positive ($n = 140$) (Supplementary Fig. 2a). More than 85% of the

Figure 1 | Structure and expression of Elfn1. (**a**) Domain structure of Elfn1. LRR, leucine rich repeat; CT, C-terminal domain; FNIII, fibronectin type-III domain; TM, transmembrane domain. (**b**) Subcellular distribution of Elfn1 in the mouse brain. H, homogenates; S1, postnuclear supernatant; P1, nuclear pellet; S2, supernatant after P2 precipitation; P2, crude synaptosomes; S3, cytosol; P3, light membrane; LP1, crude synaptosomal membranes; LP2, synaptic vesicle-enriched fraction; SPM, synaptosomal plasma membranes. (**c**,**d**) Developmental expression patterns (**c**) and regional distribution (**d**) of Elfn1 protein in mouse brain as analysed by IB. P, postnatal day; W, weeks. ob, olfactory bulb; cc, cerebral cortex; hp, hippocampus; st-gp, striatum and globus pallidus; th, thalamus; ht, hypothalamus; mb, midbrain; po, pons; cb, cerebellum; mo, medulla oblongata; sc, spinal cord. Equal amounts of protein were loaded. (**e**) Immunofluorescence staining of Elfn1 in a frozen sagittal section of adult mouse brain. cc, cerebral cortex; hpf, hippocampal formation; mfb, magnocellular basal forebrain; db, diagonal band; sn, substantia nigra. The picture at right is a magnified view of the hippocampal formation in the picture at left. SUB, subiculum; SP, stratum pyramidale; SR, stratum radiatum; SLM, stratum lacunosum moleculare; SM, stratum moleculare; H, hilus. Scale bar, left, 5 mm. (**f**–**i**) Double immunofluorescence staining of vibratome coronal sections through the dorsal hp from 4-month-old WT mouse brain with anti-Elfn1 (red) and anti-somatostatin (**f**, green, SOM) or anti-PV (**g**, green). Scale bars, 100 μm. (**h**) Percentage of double-labelled neurons as a proportion of total Elfn1-positive neurons in the respective layers. (**i**) Percentage of double-labelled neurons as a proportion of the total number of cells immunopositive for SOM or PV. Data were obtained from one hemicoronal section per animal ($n = 3$ mice). Mean values ± s.e.m. are shown. (**j**) Double immunofluorescence staining of the hippocampal CA1 and DG regions. Vibratome coronal sections from 4-month-old WT mouse brain were stained with anti-Elfn1 (magenta) and anti-mGluR1a (green). Images at bottom are magnified images of the boxed regions in the upper image. Closed arrowheads and arrows, Elfn1 + and PV + soma; open arrowheads, Elfn1 + and PV − soma. Scale bars, 20 μm for upper images and 10 μm for bottom images.

Elfn1-positive neurons were SOM-immunopositive in the CA1, CA3 and DG regions (Fig. 1f,h; Supplementary Fig. 1c). Conversely, nearly all of the SOM-positive neurons were immunopositive for Elfn1 (Fig. 1i), demonstrating that Elfn1 and SOM largely coexist in the hippocampal interneurons. In addition, around 20% to 30% of the Elfn1-positive neurons were

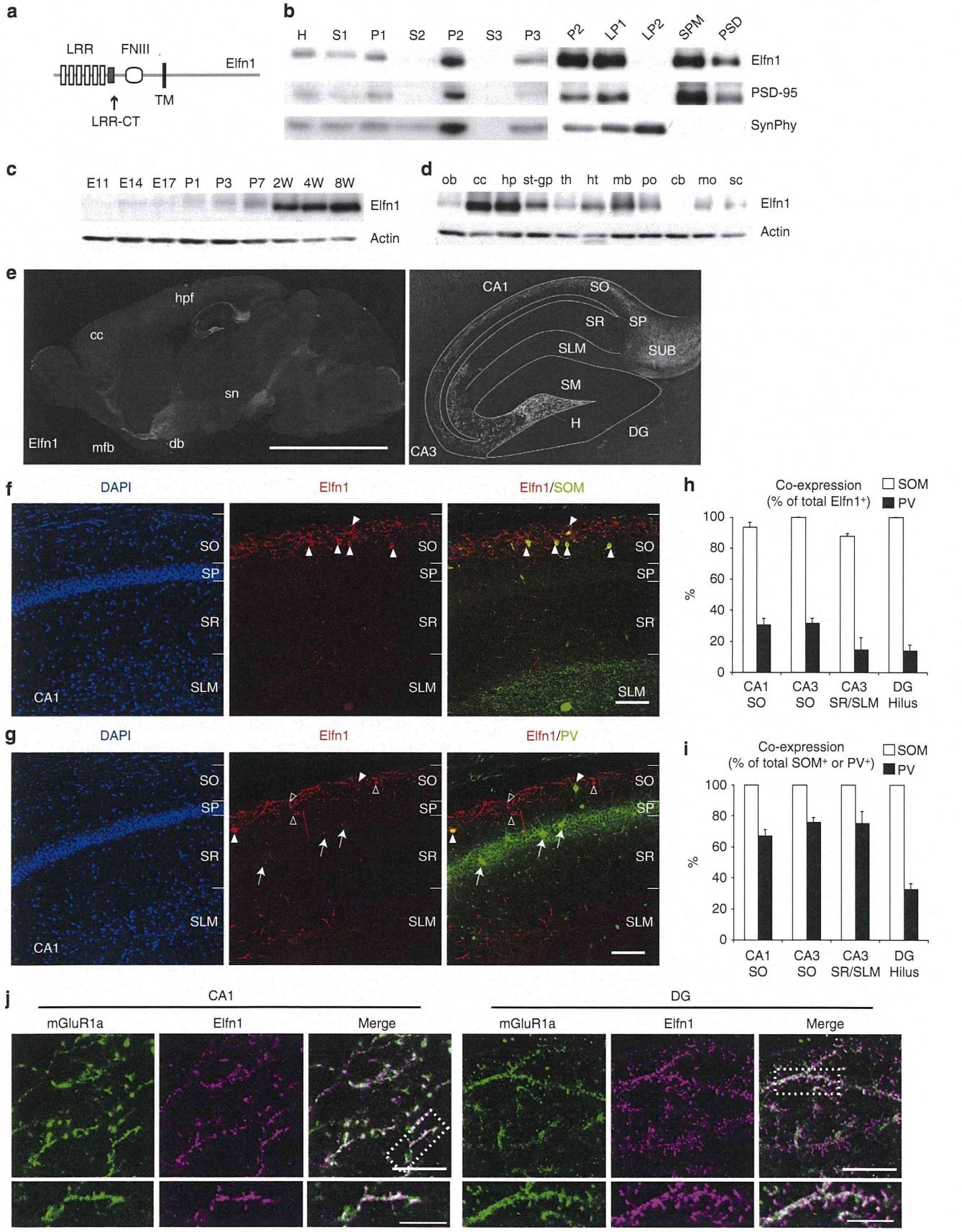

immunopositive for parvalbumin (PV) (Fig. 1g,h), suggesting that some Elfn1-positive cells express both SOM and PV.

Hippocampal SOM-INs include OLM and oriens-bistratified cells in the CA1 region and HIPP cells in the DG[7,23]. Double labelling with Elfn1 and SOM revealed SOM-positive cells with dense Elfn1 signals in the SO and hilus regions (Fig. 1f; Supplementary Fig. 1c), suggesting that Elfn1 is strongly expressed in OLM and HIPP cells. Because OLM and HIPP cells show abundant expression of mGluR1a[8,24], we performed double staining with mGluR1a and Elfn1. As expected, Elfn1 and mGluR1a signals overlapped in the CA1 and hilus regions (Fig. 1j). Some of the dendrites of Elfn1- and mGluR1a-positive interneurons in CA1 and most of the dendrites in the hilus possessed spines (Fig. 1j), which is another characteristic feature of OLM and HIPP cells.

Elfn1 recruits mGluR7 in trans. Because multiple LRR-containing transmembrane proteins possess synaptogenic properties[25], we first performed a neuron–fibroblast co-culture assay to investigate whether Elfn1 or Elfn2 expressed in non-neural cells could induce presynaptic differentiation when contacting axons of co-cultured neurons. However, unlike neuroligin-1, neither Elfn1 nor Elfn2 showed synapse-inducing activity (Supplementary Fig. 2b,c). Considering the restricted localization of Elfn1 in OLM and HIPP interneurons, we then hypothesized that Elfn1 could be involved in the regulation of synaptic proteins specific to OLM and HIPP cells. To examine this, rat hippocampal neurons were transfected 7 days after plating (7 days *in vitro*) with vectors expressing green fluorescent protein (GFP) or Elfn1 C-terminally tagged with GFP (Elfn1–GFP). Most transfected cells showed a dense distribution of Elfn1–GFP overlapping with the postsynaptic scaffold protein PSD-95, and some were adjacent to a presynaptic protein, Vglut1 (Supplementary Fig. 3a). When we immunostained the transfected cells with anti-mGluR7 and anti-mGluR1a antibodies at DIV9, Elfn1–GFP-expressing cells were decorated by mGluR7-immunopositive puncta but were negative for mGluR1a immunoreactivity (Fig. 2a; Supplementary Fig. 3a). In contrast, mGluR7 signals were scarcely detected in GFP-transfected cells (Fig. 2a). Endogenous mGluR7-immunoreactive puncta were observed in the vicinity of the GAD67-, mGluR1a- or Elfn1-positive inhibitory neurons at later stages (DIV17, Fig. 2b; Supplementary Fig. 3b; DIV51, Fig. 2c). At a higher magnification, the mGluR7 signals overlapped with the presynaptic marker Vglut1 and were adjacent to Elfn1-immunoreactive signals (Fig. 2c). To examine the induction specificity, we expressed mGluR1a–GFP or Flrt3–GFP, which is known to induce presynaptic differentiation through physical interaction with latrophilin 3, a presynaptic seven-pass transmembrane receptor[26]. However, these proteins did not recruit mGluR7, suggesting that the mGluR7-recruiting ability is specific to Elfn1 (Fig. 2a). We next expressed Elfn1, mGluR1a and Flrt3 in HEK293 cells, which do not express mGluR7, and co-cultured them with DIV13 hippocampal neurons (Fig. 2d,e). Both Elfn1 and Elfn1–GFP recruited mGluR7, whereas mGluR1a–GFP and Flrt3–GFP did not. These results suggest that Elfn1 can recruit mGluR7 in trans and that Elfn1 is sufficient for mGluR7 recruitment *in vitro*. Consistent with the absence of synaptogenic activity, most mGluR7-positive puncta induced by Elfn1 were separated from Vglut1 signals (Fig. 2e). However, when a synaptogenic molecule (neuroligin 2) was co-expressed, mGluR7 puncta signals overlapped with Vglut1, suggesting that Elfn1 can recruit mGluR7 at both synaptic and non-synaptic sites (Fig. 2e; Supplementary Fig. 3c).

Elfn1 physically interacts with mGluR7 *in vivo*. The above results led us to examine whether Elfn1 associates with mGluR7 *in vivo*. In immunoprecipitation experiments with mouse brain lysate and an anti-Elfn1 antibody, mGluR7 was co-precipitated with Elfn1 (Fig. 3a). Likewise, an anti-mGluR7 antibody co-precipitated Elfn1 (Fig. 3b).

To address whether the association of Elfn1 and mGluR7 is mediated by their direct physical interaction, we prepared Elfn1 and mGluR7 protein fragments spanning from the amino terminus to their transmembrane domains (ectodomains) as fusion proteins with an immunoglobulin Fc domain and a myc/polyhistidine tag, respectively, to form Elfn1–Fc and mGluR7–MycHis. When the Elfn1–Fc and mGluR7–MycHis were incubated for 1 h at room temperature and the Fc fusion proteins were precipitated with protein G-Sepharose, mGluR7 was co-precipitated (Fig. 3c). Co-precipitation was not observed with other reference proteins, either with Fc alone or SLITRK3 ectodomain-Fc (SLITRK3 is an LRR-transmembrane protein known to induce inhibitory synapses by interacting with a receptor protein tyrosine phosphatase, Ptprd[27]). The addition of Elfn1–Fc to the culture medium of Elfn1–GFP-transfected neurons resulted in 73% lower recruitment of mGluR7 than the addition of Fc alone (Fc, 1.0 ± 0.28; Elfn1–Fc, 0.27 ± 0.07; $P = 0.019$, unpaired t-test, $n = 12$ images, Fig. 3d). These results indicate that the transinteraction of Elfn1 with mGluR7 is necessary for mGluR7 recruitment.

mGluR7 surrounding OLM/HIPP is reduced in Elfn1 KO mice. To examine the role of Elfn1 *in vivo*, we generated *Elfn1* KO (*Elfn1*$^{-/-}$) mice by homologous recombination in ES cells (Supplementary Fig. 4a,b). The absence of Elfn1 protein was confirmed by IB and immunofluorescence staining (Supplementary Fig. 4c,d). Specific co-precipitation of mGluR7 or Elfn1 with anti-Elfn1 or mGluR7 was ensured using samples from *Elfn1* KO mice (Fig. 3a,b). There were no apparent defects in gross brain morphology (Supplementary Fig. 4e).

To examine whether the synapses on OLM or HIPP interneurons are altered in the hp of *Elfn1* KO mice, we compared the localization of mGluR7 and mGluR1a between wild-type (WT) and KO mice (Fig. 4a–e). In the hp of WT mice, mGluR7 puncta were densely associated with mGluR1a-positive signals in the outer region of CA1 (OLM in Fig. 4a) and the hilus of the DG (Fig. 4a). By contrast, the association of mGluR7 with mGluR1a-positive signals was rarely observed in KO mice in either region (Fig. 4a,b). In the DG, the KO mice had significantly fewer mGluR7-positive spines at both 9 weeks and 4 months (Fig. 4c). In other regions, such as the SO and striatum radiatum of CA1, the mGluR7 distribution did not differ between WT and KO mice (Fig. 4a,b).

Total mGluR1a levels did not differ between WT and KO mice (Supplementary Fig. 4f,g). In terms of adjacent Vglut1 signal levels, the mGluR1a-positive neurons in the SO or in hippocampal dissociated culture did not show clear genotype-dependent differences (Supplementary Fig. 5). We further investigated mGluR1a localization within the dendritic spines of WT and KO DG (Fig. 4d,e). In 9-week-old mice, the density of mGluR1a-positive spines in the DG hilus did not differ between WT and KO mice (Fig. 4e). However, at 4 months of age, KO mice showed a small but significant decrease in spine density (Fig. 4e), and the mGluR1a-positive signals within the spines were of shorter length in both 9-week-old and 4-month-old KO mice (Fig. 4d). These results indicate that Elfn1 deficiency does not clearly influence synapse formation itself. Taken together with the *in vitro* experiments, the analysis of *Elfn1* KO mice corroborated the role of Elfn1 as a transregulator in recruiting mGluR7 (Fig. 4f).

We also examined the distribution of Elfn1 and mGluR7 proteins in younger mice. Both Elfn1- and mGluR7-positive

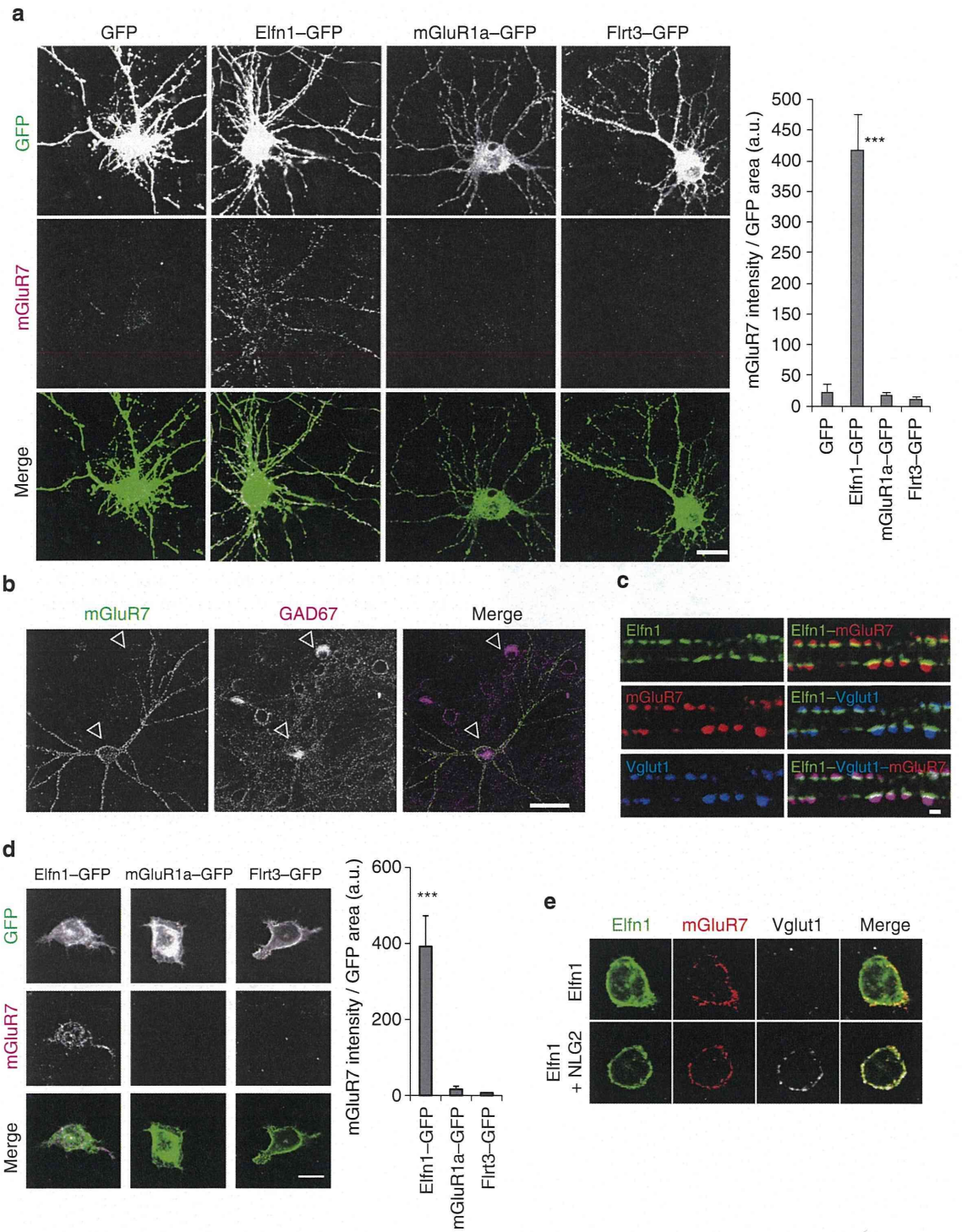

Figure 2 | Elfn1 recruits mGluR7. (**a**) Elfn1-GFP can recruit mGluR7 signals. Dissociated hippocampal neurons were transfected with Elfn1-GFP, mGluR1a-GFP, Flrt3-EGFP or EGFP expression constructs at 7 days *in vitro* (DIV7). The cells were fixed at DIV9 and immunostained for mGluR7. Scale bar, 20 μm. Graph at right, quantification of mGluR7 intensity normalized to GFP area. a.u. arbitrary unit ***$P<0.001$, compared with GFP, unpaired *t*-test. $n=24$ for GFP, $n=23$ for Elfn1-GFP, $n=24$ for mGluR1a-GFP and $n=21$ for Flrt3-GFP from four independent cultures. (**b**) Endogenous mGluR7 signals were clustered on inhibitory neurons. Untransfected hippocampal neurons were fixed at DIV17 and double stained for mGluR7 (green) and GAD67 (magenta). Arrowhead indicates the position of the GAD67-positive cell body in each panel. Scale bar, 50 μm. (**c**) Triple immunolabeling of endogenous Elfn1 (green), mGluR7 (red) and Vglut1 (blue) in untransfected hippocampal neurons at DIV51. mGluR7 signals overlapped with Vglut1 and were adjacent to Elfn1 signals. Scale bar, 1 μm. (**d**) Elfn1-GFP-transfected HEK293 cells can also recruit mGluR7 signals. Elfn1-GFP transfectants, mGluR1a-GFP transfectants and control Flrt3-GFP transfectants were laid on top of DIV13 hippocampal neurons. Scale bar, 20 μm. The mGluR7 signals in the GFP-positive area were quantified densitometrically (graph at right; a.u.). ***$P<0.001$, compared with Flrt3-GFP, unpaired *t*-test. $n=7$ for Elfn1-GFP, $n=15$ for mGluR1a-GFP and $n=18$ for Flrt3-GFP. (**e**) Elfn1-GFP-expressing HEK293 cells can recruit Vglut1-independent mGluR7 signals while the co-expression of neuroligin 2 (NLG2) can attract mGluR7 signals that partially overlap with Vglut1.

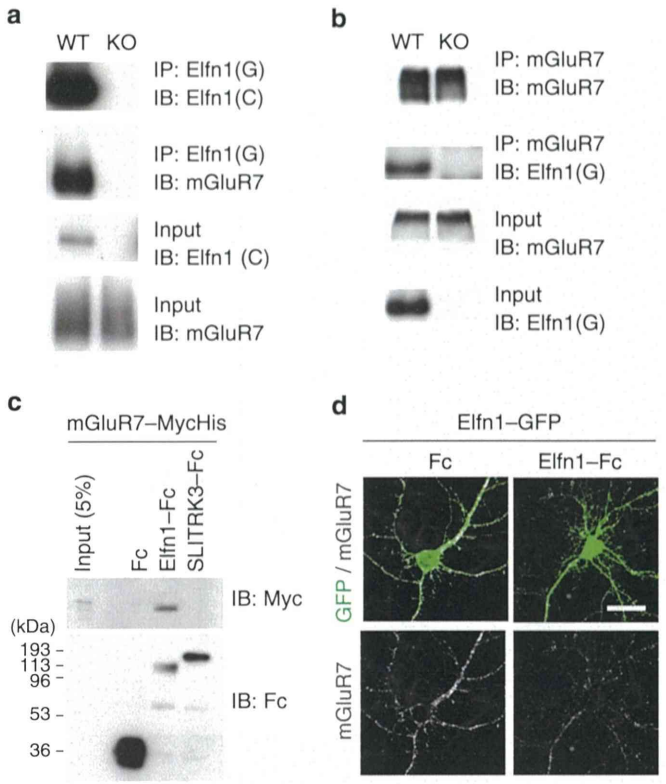

Figure 3 | Elfn1 binds mGluR7. (**a**,**b**) Immunoprecipitation using an anti-Elfn1 antibody (**a**) and anti-mGluR7 antibody (**b**). WT and Elfn1 KO brain lysates were subjected to immunoprecipitation (IP) analysis. The co-precipitated mGluR7 (**a**) and Elfn1 (**b**) were detected with IB using specific antibodies. G, antibody against the entire cytoplasmic region of Elfn1; C, antibody against the C-terminal 12 residues. (**c**) Purified Elfn1 ectodomain can bind the mGluR7 ectodomain. Bare Fc protein, Elfn1-Fc protein, SLITRK3-Fc protein and mGluR7-MycHis protein were produced in HEK293 cells and each protein was affinity purified. Fc proteins and mGluR7-MycHis were mixed, and Fc proteins were precipitated with protein G-Sepharose. Precipitated mGluR7-MycHis and Fc proteins were detected with an anti-Myc epitope antibody and anti-Fc antibody, respectively. Blots are representative of at least two biological replicate experiments. (**d**) Addition of purified Elfn1 ectodomain inhibits the recruitment of mGluR7 in Elfn1-GFP-transfected neurons. Bare Fc or Elfn-Fc proteins were added to the culture media of Elfn1-GFP-transfected neurons at DIV8, which were immunostained for mGluR7 after 36 h. Scale bar, 20 μm.

signals were detected in partially overlapping regions of WT hippocampi at embryonic day (E) 16, postnatal day 0, P3 and P7 (Supplementary Fig. 6; Fig. 4g,h). At P3, there were strongly Elfn1-positive and mGluR7-positive signals at the prospective SO layer in WT mice (Supplementary Fig. 6; Fig. 4g). Double labelling revealed that the two signals were partially overlapping (Fig. 4g). At P7, the corresponding mGluR7 signal was detected in WT but not in KO mice (Fig. 4h). These results indicate that Elfn1 is required for the recruitment of mGluR7 starting in the early postnatal period.

Presynaptic form of plasticity is impaired in KO synapses. A previous study revealed that viral vector-mediated *Elfn1* knock-down alters the presynaptic form of short-term plasticity of CA1 pyramidal neuron–OLM synapses[21]. To clarify the role of Elfn1 in presynaptic functions *in vivo*, we recorded excitatory postsynaptic currents (EPSCs) from OLM (Fig. 5a) and pyramidal neurons in WT and KO mice and studied the presynaptic form of plasticity. A brief burst stimulation of afferents from CA1 pyramidal neurons induced large short-term facilitation at excitatory synapses onto OLM neurons in WT mice (Fig. 5b; $n=9$ from three mice). By contrast, synapses in KO mice did not show facilitation, and the third, fourth and fifth EPSCs were even depressed (Fig. 5b; $n=12$ from two mice; 10 Hz, second EPSC, $P=0.0054$, third, $P=0.0050$, fouth, $P=0.0020$, fifth, $P=0.0023$; 20 Hz, second, $P=0.031$, thirdrd, $P=0.014$, fourth, $P=0.019$, fifth, $P=0.014$, unpaired t-test), suggesting that deleting Elfn1 elevates release probability and impairs short-term plasticity at excitatory synapses onto OLM neurons. In contrast, short-term plasticity of synaptic inputs to pyramidal neurons, used as a reference, was comparable between WT and KO mice (Fig. 5c,d; WT, $n=15$ from two mice; KO, $n=13$ from two mice), indicating that Elfn1 selectively regulates short-term plasticity at synapses onto OLM neurons. We also investigated long-term potentiation (LTP) at CA1 pyramidal neuron–OLM synapses, which has been reported to be expressed presynaptically[28]. Theta burst stimulation (TBS, see Methods) at −70 mV induced robust LTP of excitatory postsynaptic potentials (EPSPs) in WT mice; however, LTP was much smaller, and long-term depression was even induced by TBS in some OLM neurons in KO mice (Fig. 5e; WT, 402.5% ± 78.8% of baseline 40 min after TBS, $n=11$ from 10 mice; KO, 116.1% ± 16.6%, $n=10$ from 7 mice; $P=0.0045$; unpaired t-test). To assess the site of expression of this plasticity, we analysed the CV (coefficient of variation , a ratio of s.d. to mean) of EPSPs before and 40 min after TBS[29]. The normalized CV^{-2} of EPSPs after TBS was higher than the normalized mean EPSP amplitude after TBS in OLM neurons in which LTP was induced, and lower than the normalized means in neurons in which long-term depression was induced (Fig. 5f), suggesting that long-term changes induced in OLM neurons were presynaptically expressed. Thus, Elfn1 reduces release probability at pyramidal neuron–OLM neuron synapses while preserving the presynaptic form of LTP and short-term facilitation.

Sensory-triggered seizures in *Elfn1* KO mice. To investigate higher brain function abnormalities caused by *Elfn1* deficiency, we investigated the *Elfn1* KO mice at an individual level. *Elfn1* KO mice were born at the expected Mendelian ratios (WT, 26.6%; heterozygote, 47.2%; KO, 26.2%; $n=778$) and the mutation was not lethal. There were no body weight differences at 6 months of age (WT, 33.2 ± 1.2 g, $n=7$; KO, 33.4 ± 1.2 g, $n=12$; male mice).

Notably, however, we frequently observed seizure-like behaviours of the adult *Elfn1* KO mice during routine handling when changing cages (Fig. 6a; Supplementary Movie 1). To assess their susceptibility to handling-induced seizures, the mice were left undisturbed for 2 weeks before testing, and on the test day, they were picked up by their tail and immediately placed in a new cage. The mice exhibited behavioural signs such as loss of postural equilibrium, Straub tail (arrow in Fig. 6a), excessive salivation and tonic convulsions during the 2-min observation period; that is, they showed epileptic phenotypes. Handling-induced seizures were observed beginning at 11 weeks after birth (Fig. 6b), and the percentage of affected animals peaked (at about 80%) at 5 months (Fig. 6b; Supplementary Table 1). The handling-induced seizures were observed in both male and female *Elfn1* KO mice, but were never observed in WT or *Elfn1* heterozygous littermates (Supplementary Table 1).

To further evaluate the seizure-prone phenotypes of *Elfn1* KO mice, seizure susceptibility was examined by using pentylenetetrazole (PTZ, a $GABA_A$ receptor antagonist) as a convulsant. At 6 months, 4 (57%) of 7 WT and 11 (92%) of 12 KO mice showed generalized seizures within 600 s after an intraperitoneal